



Research article

Parabolic transport measurement of hydrodynamic forces for flow around circular/triangular distance dependent obstructions: Finite element analysis

Khalil Ur Rehman^{1,2,*}, Wasfi Shatanawi^{1,3}, Kamal Abodayeh¹ and Taqi A.M. Shatnawi³

¹ Department of Mathematics and Sciences, College of Humanities and Sciences, Prince Sultan University, Riyadh 11586, Saudi Arabia

² Department of Mathematics, Air University, PAF Complex E-9, Islamabad 44000, Pakistan

³ Department of Mathematics, Faculty of Science, The Hashemite University, P.O. Box 330127, Zarqa 13133, Jordan

* **Correspondence:** Email: kurrehman@psu.edu.sa.

Abstract: The present effort is the low Reynolds finite element hybrid meshed solution to apprehend the flow field properties in a convergent-divergent (CD) domain having engineering standpoints applications. To be more specific, we have considered the CD domain rooted with two types of obstructions in three various arrangements namely triangular/triangular, circular/triangular, and triangular/circular in CD throat. The viscous fluid is introduced from the inlet and interacts with installed obstacles. The moving stream in the channel is modelled mathematically in terms of the two-dimensional time-independent equations. The finite element approach is used to disclose numerical solutions by means of a hybrid meshing scheme. Optimized drag and lift force values encountered by an obstruction are offered through line integration across the external obstruction surfaces. In comparison to obstruction in left vicinity, the lift force faced by the triangle obstacle on the right side of the CD throat is larger. Furthermore, as compared to the drag force faced by the triangular obstruction in the same proximity, the circular obstacle experienced greater values as a drag. The lifting force sensed by the triangular cylinder is larger than circular cylinders. The assessment of marine hydrodynamic forces and stability individualities for fully or partially submerged objects in ocean engineering will benefit from the results of this study.

Keywords: fractional distance; hydrodynamic forces; nonlinear PDEs; newtonian model;

triangular/circular obstructions; CD domain; hybrid meshing

Mathematics Subject Classification: 35A25, 65M06, 76D05

Nomenclature

x, y	Space variables
u, v	Velocity components
ρ	Fluid density
ν	Kinematic viscosity
h	Height of the channel
L	Characteristic length
Re	Reynolds number
U	Reference velocity
u_{max}	Inflow maximum velocity
D_F	Drag force
D_c	Drag coefficient
L_F	Lift force
L_c	Lift coefficient

1. Introduction

The fluid flow around obstacles is a topic of great interest because of its numerous engineering applications. The obstacles may include the shape of rectangular, triangular, square, or circular. Such obstacles are used in naval, civil, and mechanical engineering like heat exchangers (chimneys), bridge piers, power lines, and onshore/offshore platforms to mention just a few. Therefore, fluid flow around obstacles like rectangular, triangular, square, and circular is considered a fundamental problem of fluid mechanics. The flow around obstacles admits various physics phenomena namely vortex shedding in case of time-dependent flow, flow separation, turbulence, drag force, and lift force. To evaluate such characteristics, different important computational analyses were reported by researchers like Gerrard [1] examined fluctuating pressure on the cylinder as an obstacle for a certain range of Reynolds numbers to determine the lift and drag on circular cylinders. For higher Reynolds numbers, the fluctuating drag component was calculated and found to be orders of magnitude smaller than the lift. Kacker et al. [2] evaluated the lift forces that cylinders with various diameters and length-to-diameter ratios encountered towards different Reynolds numbers. The fluctuating drag and lift coefficients for length-to-diameter ratios were calculated by combining data from stations across a horizontal section of the tube that measure the changing surface pressure. Lift coefficients for cylinders were matched with the experimental study, with the values taken by surface pressure at lower Reynolds numbers. Gerrard [3] studied the flow around circular cylinders, and he also noted the wakes of bluff cylinders with various cross sections. The research mostly focuses on using a dye that has been removed from the bodies to visualize the movement of wakes. Therefore, the dye patterns seen were filament line demonstrations of the flow leaving the body's separating lines. Because vorticity diffuses much more quickly than dye at low Reynolds numbers, it has been noticed that the dye does not render the vorticity-bearing fluid visible. Norberg [4] studied the impacts of the Reynolds number in the nominal situation of a large aspect-ratio cylinder at minor to vanishing obstruction, specific elements of the

fluctuating lift force on a stationary circular cylinder. They came to the conclusion that the lift fluctuations on a finite length of the cylinder were therefore reliant on both the spanwise correlation of the lift-related flow and the sectional lift changes. For higher Reynolds numbers, Catalano et al. [5] studied the flow around a circular cylinder in the supercritical domain. For the large-eddy simulation's estimated boundary conditions, a straightforward wall stress model was used. The outcomes were contrasted with experimental data and results from stable and unsteady Reynolds-averaged Navier-Stokes solutions. Following the drag crisis, they accurately depict the delayed boundary layer separation and decreased drag coefficients corresponding with experimental results. Since then many researchers explored flow around obstacles see Refs. [6–11]. Zhao et al. [12] provided a three-dimensional numerical simulation of sinusoidal oscillatory flow around a circular cylinder at oblique and right attacks. Oblique angle calculations and Reynolds number calculations were performed. For single-mode flows, the spanwise correlation factor determined using the sectional transverse force was close to 1. In general, the correlation length of multi-mode flows is less than that of single-mode flows and varies on the KC number. There was discussion about both the maximum lift coefficient and the mode-averaged lift force disparities. Sami [13] examined the velocity field of two-dimensional turbulent flow about a partially buried circular cylinder on a smooth plane boundary. Experiments were conducted in a closed-loop water channel with diameter-dependent Reynolds numbers. The positions of the separation points on the surface of an obstacle as well as the influence of the burial ratio downstream and separation upstream were examined. Yu et al. [14] developed a two-dimensional model for the flow through a circular patch containing a collection of vertical circular cylinders. The model's applicability was initially verified through test situations where experimental data could be compared with the calculated outcomes. The ability of the current model to accurately forecast average velocity and turbulence structure has been confirmed. Then, using the current model, the drag coefficient was determined for a variety of scenarios with various cylinder Reynolds numbers, solid volume fractions, and patch diameters. It was demonstrated that the drag coefficient lowers with an increase in Reynolds number but increases with an increase in solid volume fraction. The flow past a circular cylinder at a crucial Reynolds number was explored by Lehmkuhl et al. [15] It was shown that as the Reynolds number increases, the pressure distribution changes asymmetrically, first on one side of the cylinder and subsequently on the other side to complete the drag reduction. Mehdi et al. [16] investigated the fluid flow around a circular, two-dimensional obstacle with various Reynolds numbers. A second-order implicit scheme and implicit pressure-based finite volume approach were employed in this simulation. Equations for Navier-Stokes and continuity were used to study flow. For various Reynolds numbers and varying angles of attack, the pressure, drag coefficients, and vortex shedding were calculated and compared with previous numerical results that show good agreement. Experimental research on the characteristics of flow around a modified circular cylinder was done by Gao et al. [17] In a wind tunnel, the experimental campaign was carried out at a high Reynolds number. A slit parallel to the entering airflow was added to the cylindrical test model to create a flow communication route between the windward and leeward stagnation regions. The findings of the experiment show that a slit helps to lower the drag and decrease the varying amplitude of the dynamic wind loads operating on the test model. The shifting trend in lift suppression and drag reduction with the expansion of the slit width was also covered. Bao [18] solved the Navier-Stokes equations numerically for a circular cylinder with a slit. At a Reynolds number, they applied the high-resolution spectral element approach. The results demonstrate that for attack angle, a higher slit width ratio and a lower attack angle are generally likely to produce a lower root-mean-square lift coefficient. For each slit width ratio, the mean drag coefficient and root-mean-square lift coefficient were higher than those of a typical cylinder. It was discovered that the vortices are stronger and more stable than a typical cylinder.

Motivated by the literature reported above on the significance of flow around obstacles, we offer a numerical evaluation of hydrodynamic forces in this article by considering regular obstructions with fractional distance towards an ongoing fluid in convergent-divergent channel. It is important to note that in this manuscript the word “fractional” refers (only) to distance measurement. We are confident that by following the present article one can learn the initial step towards evaluating hydrodynamic forces having importance in daily life like the presence of ships, energy converters by wave, offshore rigs, and sub-surface pipelines resulting in hydrodynamic forces such as drag and lift. The investigators face difficulty in evaluating such hydrodynamics forces in diverse combinations. Therefore, the present attempt is the numerical catalyst to study fluid stream in CD domain having triangular/triangular, circular/triangular, and triangular/circular obstacles. The article is carried out as: Section-1 is for current and past quantitative analysis on the flow around obstacles, along with various physical findings. The steady Navier-Stokes equations that narrate the flow around obstacles in the CD channel are framed in Section-2. The relation for concerned forces is given in Section-3. The numerical simulation directory is offered in Section-4. Section-5 offered a comparative examination of the flow. Section-6 includes the key findings of the present analysis of drag and lift forces faced by triangular/triangular, circular/triangular, and triangular/circular. One can extend the study for evaluation of hydrodynamic forces having ocean engineering standpoints see Refs. [19–21].

2. Mathematical description of CD flow

Motivated by Schaefer et al. [22] on flow in a channel having a circular obstacle, we consider convergent-divergent channel of dimensions $\Gamma: [0, 1.6] \times [0, 0.6]$ with the installation of triangular and circular cylinders in right/right vicinity of the CD throat. The velocity of flow at every point is parallel to a fixed $x - y$ plane as a two-dimensional flow. The geometry of the problem is offered in Figure 1. The boundary condition of the CD channel is as follows:

- **Upper/Lower walls:** We carried no-slip condition. Mathematically such assumption is written as: $v = 0, u = 0$.
- **Inlet of channel:** The viscous fluid flow is initiated with fully developed parabolic inflow velocity. Mathematically such assumption is written as: $u = 4u_{max}$. The compatibility of the parabolic profile instead of the linear with the no-slip assumption is debated in Refs. [23,24].
- **Outlet of channel:** The “do nothing condition” is applied at the outlet of the channel. Mathematically it is written as $u_x = 0, v_x = 0$. In addition, the outer surfaces of circular and triangular obstructions are also carried with no-slip condition.

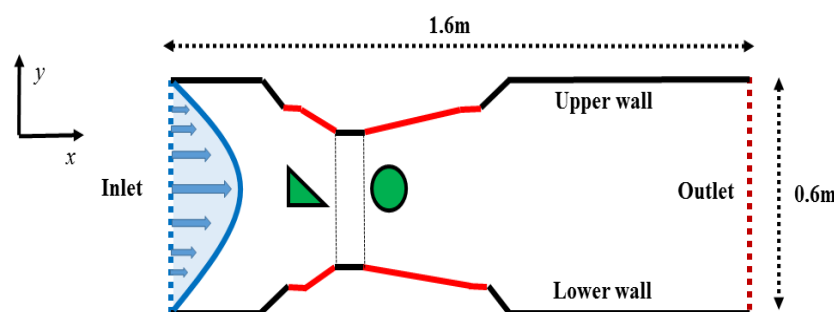


Figure 1. Triangular/circular obstacles with in CD domain.

The interaction of a steady Newtonian continuous stream with installed obstructions in the CD channel can be studied by the differential equations known by the continuity equation and low Reynolds time-independent Navier-Stokes equations:

$$\frac{\partial u_i}{\partial x_i} = 0, \quad (1)$$

$$u_j \frac{\partial u_i}{\partial x_j} = -\frac{1}{\rho} \frac{\partial p}{\partial x_i} + \nu \frac{\partial^2 u_i}{\partial x_j^2}. \quad (2)$$

For results generalization or be an abstract over a wide range of phenomena we need to obtain dimensionless forms. For this purpose, one can use

$$\bar{u}_i = \frac{u_i}{U}, \bar{x}_i = \frac{x_i}{L}, \bar{p} = \frac{p}{\rho U^2}, Re = \frac{UL}{\nu}, \quad (3)$$

by using Eq (3) we reached at:

$$\frac{\partial \bar{u}_i}{\partial \bar{x}_i} = 0, \quad (4)$$

$$\bar{u}_j \frac{\partial \bar{u}_i}{\partial \bar{x}_j} = -\frac{\partial \bar{p}}{\partial \bar{x}_i} + \frac{1}{Re} \frac{\partial^2 \bar{u}_i}{\partial \bar{x}_j^2}, \quad (5)$$

by removing the bar we get the following forms in terms of steady velocity components:

$$\frac{\partial u_i}{\partial x_i} = 0, \quad (6)$$

$$u_j \frac{\partial u_i}{\partial x_j} = -\frac{\partial p}{\partial x_i} + \frac{1}{Re} \frac{\partial^2 u_i}{\partial x_j^2}, \quad (7)$$

Eqs (6) and (7) in terms of velocity components can be written as:

$$\frac{\partial u}{\partial x} + \frac{\partial v}{\partial y} = 0, \quad (8)$$

$$u \frac{\partial u}{\partial x} + v \frac{\partial u}{\partial y} = -\frac{\partial p}{\partial x} + \frac{1}{Re} \left(\frac{\partial^2 u}{\partial x^2} + \frac{\partial^2 u}{\partial y^2} \right), \quad (9)$$

$$u \frac{\partial v}{\partial x} + v \frac{\partial v}{\partial y} = -\frac{\partial p}{\partial y} + \frac{1}{Re} \left(\frac{\partial^2 v}{\partial x^2} + \frac{\partial^2 v}{\partial y^2} \right). \quad (10)$$

3. Hydrodynamic forces in CD channel

The quantity of interest namely “variation in hydrodynamic forces” is appeared when we have installed two various obstacles in CD channel. Particularly, triangular/triangular, triangular/circular, and circular/triangular obstacles in the CD channel experienced lift perpendicular and drag parallel to the flow. All of the complicated dependencies of shape, flow conditions and angle of attack are modeled by using drag and lift coefficients [22–24]. Therefore, to evaluate such coefficients for each obstruction we used mathematical relations as follows:

$$L_c = \frac{2L_F}{\rho(U)^2 L}, \quad (11)$$

$$D_c = \frac{2D_F}{\rho(U)^2L}. \quad (12)$$

Here, lift coefficient relation is given as Eq (11) and drag coefficient relation is offered in Eq (12). For simulation we considered viscosity velocity $\mu = 0.001$, Newtonian fluid density $\rho = 1$, $U = 0.2$ as reference velocity, and $L = 0.1$ as a character length. One should note that for triangular obstacle we consider the side of triangular as a characteristic length while for circular obstacle we own the diameter of the cylinder as a characteristic length $L = 0.1$. The coefficients namely drag and lift are calculated by performing line integration around triangular/triangular, triangular/circular, and circular/triangular obstacles in CD channel at $Re = 20$.

4. Numerical solution scheme

The flow narrating equations namely continuity and Navier-Stokes equations are given in Eqs (1) and (2) respectively. We need to obtain the dimensionless form therefore we used Eq (3). Use of Eq (3) results in Eqs (4) and (5). Since we have considered a two-dimensional time-independent Newtonian flow with triangular/triangular, triangular/circular, and circular/triangular obstacles in CD throat therefore the component form of Eq (5) can be used. Eqs (8)–(10) are ultimate component forms in this direction. The use of proper primitive variables results in Eqs (8)–(10) along with key dimensionless Reynolds number Re . Here we seek the solution of Eqs (8)–(10) to narrate the flow field having case-wise interaction with triangular/triangular, triangular/circular, and circular/triangular obstructions in CD throat. For the solution of fluid flow narrating differential equation we have numerous numerical and analytical methods namely adomian decomposition method (ADM), variational iterative method (VIM), Homotopy [25], perturbation method [26], finite difference, finite element method [27] and finite volume method to name a few. Each of these schemes has some restrictions that depend on convergence with accuracy. We used the Comsol Multiphysics application [28–30] on Windows® to implement the finite element technique (FEM) for solution of our flow equations. Further Q_2 (biquadratic element) and P_1^{Disc} (piecewise linear discontinuous element) are considered for spaces discretization of velocity and pressure respectively. The nine (9) and three (3) degrees of freedom (DOFs) are slotted for velocity and pressure respectively. The Q_2/P_1^{Disc} considered as stable finite element. Newtons approach is used to construct the nonlinear block system as a nonlinear solver. An iteration comes to an end, when the following relation holds:

$$\left| \frac{\lambda^{n+1} - \lambda^n}{\lambda^{n+1}} \right| < 10^{-6}, \quad (13)$$

where λ is general solution component. We used FEM along with a hybrid meshed structure to report acceptable solutions. For discretization of the domain, six various hybrid meshing levels are owned by considering triangular and rectangular elements. The involved hybrid meshing levels include Q-6, Q-5, Q-4, Q-3, Q-2, and Q-1 for all case-wise installation of obstacles. It is important to note that for all cases, the findings are grid independent at Q-6, therefore, we performed all simulations at that level Q-6. For triangular/triangular hitch in the channel, we discretized the computational domain with 103 boundary elements (BEs) and 781 domain elements (DEs). This discretization is termed as hybrid meshing level Q-1. The discretization improved by introducing 132 BEs and 1148 DEs and known as Q-2. The detail of meshing levels namely Q-3, Q-4, and Q-5 for triangular/triangular installation is accessible in Table 1. The last level is named Q-6 and in this level, we used 367 BEs and 8049 DEs. For triangular/triangular case, the simulation is performed at level Q-6 with $Re = 20$. In the second case, the circular/triangular

obstructions are carried. Q-6, Q-5, Q-4, Q-3, Q-2, and Q-1 are six level used as meshing. We discretized convergent-divergent channel rooted with circular/triangular obstructions by using 96 BEs and 708 DEs. Such discretization is known as Q-1 hybrid meshing. The improved meshing detail for Q-5, Q-4, Q-3, and Q-2 is offered in Table 2. The simulation is accomplished at hybrid meshing level Q-6 to inspect the fluid flow field around circular/triangular shaped obstructions in the CD channel. In the third case, we have considered triangular/circular shaped obstructions in convergent-divergent channel.

To inspect the flow field we have considered six different levels Q-1,2,3,4,5 and Q-6. In the first level, the domain contains 97 BEs and 713 DEs. The meshing is improved for the case when we have triangular/circular shaped obstructions in the CD channel and detail in this regard is offered in Table 3 as level Q-2, Q-3, Q-4, and Q-5. The simulation is performed at level Q-6. At this level, we own 343 BEs and 7081 DEs. We considered line integration to note the hydrodynamic forces experienced by installed obstructions. For all three events, we have also offered DOFs and central processing unit (CPU) time.

Table 1. Mesh refinement for triangular/triangular as an obstructions.

Levels (Q)	BEs	DEs	DOFs	CPU time (s)
1	103	781	1524	07
2	132	1148	2199	10
3	170	1788	3312	09
4	235	3187	5676	10
5	299	4933	8559	14
6	367	8049	13503	15

Table 2. Mesh refinement for circular/triangular as an obstructions.

Levels (Q)	BEs	DEs	DOFs	CPU time (s)
1	96	708	1407	12
2	124	1048	2034	10
3	161	1657	3099	08
4	224	2966	5319	11
5	278	4308	7554	10
6	339	7035	11886	13

Table 3. Mesh refinement for triangular/circular as an obstructions.

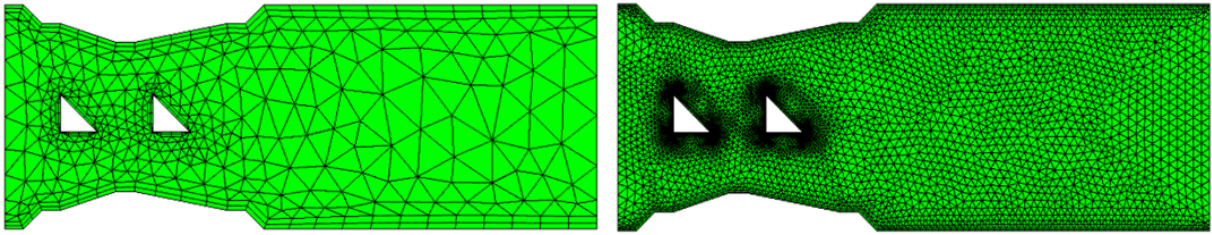
Levels (Q)	BEs	DEs	DOFs	CPU time (s)
1	97	713	1413	13
2	125	1045	2031	13
3	163	1649	3090	11
4	226	2996	5367	11
5	281	4361	7638	11
6	343	7081	11961	13

5. Comparative analysis

We have considered a convergent-divergent channel having Newtonian fluid. The fluid interaction with case-wise installation namely triangular/triangular, circular/triangular, and triangular/circular obstructions is debated numerically. The quantities of interest for each case include, drag coefficient, lift coefficient, pressure, and velocity.

5.1. EVENT-I. Triangular/triangular as an obstruction in CD throat

In this event, we considered a triangular shaped obstruction in the sides of the CD channel throat. The flowing fluid strikes with installed obstacles. The interaction is studied by using a numerical scheme. The hybrid meshing for levels namely Q-1 and Q-6 for triangular/triangular hitches in CD throat is given in Figure 2. For accuracy, the simulation is done at hybrid level Q-6. Figures 3 and 4 offer the pressure and velocity distributions around the triangular/triangular obstacles. Particularly, Figure 3 depicts the pressure outcomes for event-I. The pressure is noticed maximum towards the left of the obstacle. Down the stream the pressure variation is linear. The corresponding velocity distribution around the triangular obstruction is offered in Figure 4. The fluid hits with the first triangular obstacle and such interaction brings bifurcation and this bifurcation travels towards the second installed triangular obstacle. The obstructions impact on fluid reduces down the channel. Here line graph scheme is executed to report the flow interaction with obstruction at several positions of the CD channel see Figure 5. In detail, Figure 5 offers the trend of u -velocity of viscous fluid at inlet ($x = 0.0$), channel positions $x = 0.6, 0.7$ and 1.5 . For $x = 0.0$, one can see that the parabolic graphical trend validates the supposition of parabolic entrance of fluid from an inlet. For the viscous fluid u -velocity at channel position $x = 0.6$, the impact of installed obstacle is visible in terms of gain in fluid velocity. For u - at channel location $x = 0.7$, the u -velocity at this location is slightly less as compared $x = 0.6$. The variation in u is also witnessed at channel location $x = 1.5$. One can see that the impact of an installed obstructions reduces at the large frame and u -velocity declines significantly. The placement of triangular obstacles in the CD channel results in two forces. Such values are obtained at six various meshed levels namely Q-1,2,3,4,5 and 6. Table 4 reports the forces faced by triangular/triangular hitches. At meshing level Q-1, the lift coefficient for triangular obstruction in the left locality of CD throat is observed $L_c = 0.48980$ and drag coefficient is noticed $D_c = 10.002$. The value of lift coefficient at meshing level Q-1 for obstacle in right of CD throat is recorded $L_c = 1.0587$ and $D_c = 4.9927$. The coefficients are optimized and outcomes in this direction are shared in Table 4 subject to various meshing levels. The level Q-6 owns trustful values of coefficients. The $L_c = 0.24370$ and $D_c = 9.0756$ are optimized values of left obstacle. At level Q-6, the triangular obstruction fitted in right vicinity of CD throat own drag coefficient value $D_c = 4.3776$ and lift coefficient is noticed $L_c = 0.90197$. The drag coefficient in the left side of the throat is noticed higher in comparison to right vicinity. The opposite is the case subject to lift coefficient values.



Hybrid meshing level Q-1.

Hybrid meshing level Q-6.

Figure 2. Meshing scheme for Event-I.

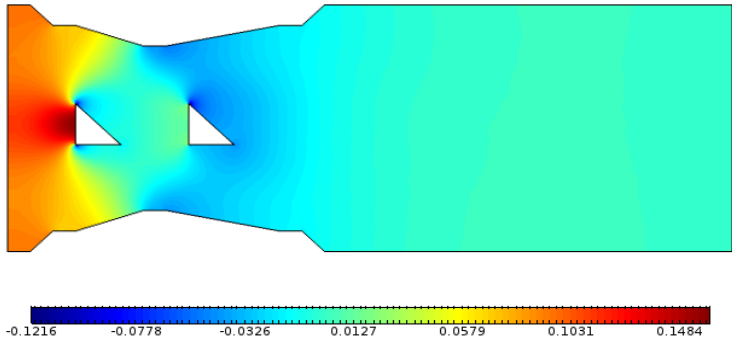


Figure 3. Pressure for triangular/triangular event.

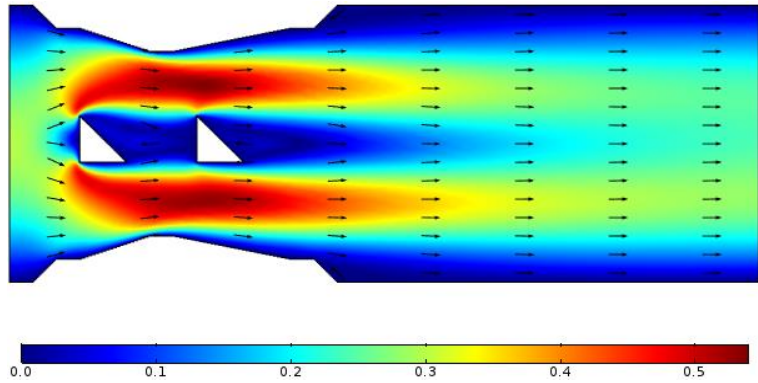


Figure 4. Velocity for triangular/triangular event.

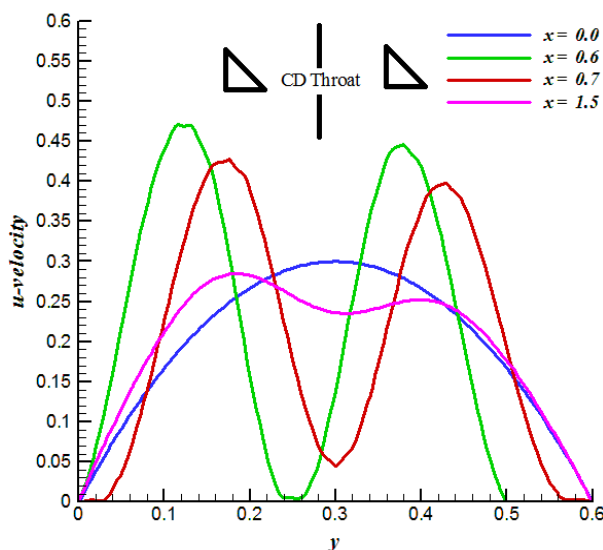


Figure 5. Line graph study for triangular/triangular event.

Table 4. Coefficients for triangular/triangular event.

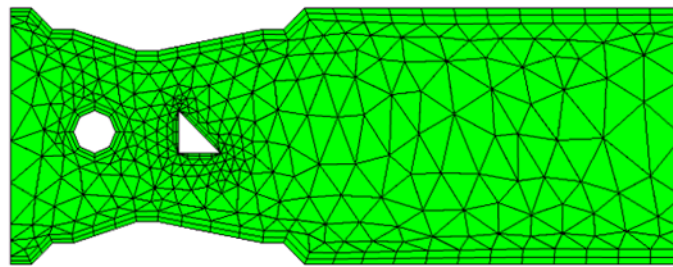
Levels (Q)	Triangular cylinder in left vicinity		Triangular cylinder in right vicinity	
	Lift	Drag	Lift	Drag
1	0.48980	10.002	1.0587	4.9927
2	0.31378	9.5195	0.99793	4.9642
3	0.29644	9.3882	0.98832	4.5755
4	0.27296	9.1636	0.94573	4.4239
5	0.25228	9.1152	0.92602	4.4181
6	0.24370	9.0756	0.90197	4.3776

5.2. EVENT-II. Circular/triangular as an obstruction in CD throat

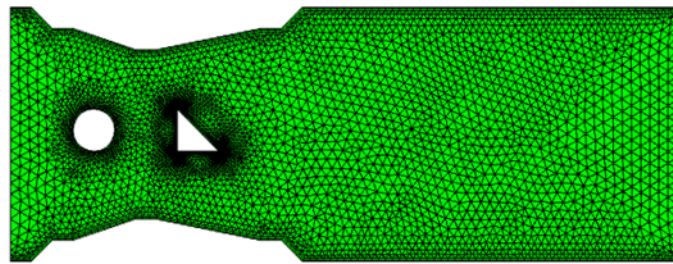
In this event, circular/triangular shaped obstructions were considered in the left/right locality. The fluid arrives with a parabolic form from the left wall of the CD channel and interacts with obstacles mounted. The relation is analyzed using the methodology of finite element method. For circular/triangular hitches in the CD throat, hybrid meshing for Q-1, and Q-6 levels is given in Figure 6. The recognition of triangular and rectangular components supports hybrid meshing. The simulation is executed at hybrid stage Q-6 for accuracy. Figures 7 and 8 provide the distribution of pressure and velocity across the circular/triangular obstructions in the CD throats left/right vicinity. Particularly, Figure 7 illustrates the distribution of pressure in a domain with a circular obstruction. It is found that the pressure on the left face of the circular obstacle is optimum. The intensity changes in a linear way down the CD channel stream. The corresponding velocity distribution in CD throat around circular/triangular obstructions is given in Figure 8.

Such contact brings bifurcation and this bifurcation near inlet gain momentum towards outlet. The influence of these obstructions on the flow of fluid decreases down the drain. The line graph analysis is also conducted to disclose separate locations ($x = 0.0, 0.6, 0.7,$ and 1.5) of the CD channel to the flow contact with obstruction. Figure 9 in this direction is plotted. For the pattern of viscous fluid u -velocity at the inlet ($x = 0.0$) of the channel, one can see that the parabolic graphical pattern

validates the belief that fluid from an inlet is parabolically reached. For channel location $x = 0.6$, the influence of the obstacle is noticeable. The u -velocity at channel location $x = 0.7$ is given in Figure 9 as well. At channel position $x = 1.5$, the difference in u -velocity is noted. We can see that the influence of mounted obstructions decreases at wide frames and u -velocity decreases. Six separate mesh sizes, namely Q-1,2,3,4,5, and Q-6, are used to achieve lift and drag coefficients. Table 5 tracks the drag and lift forces in CD throat encountered by circular/triangular obstructions. For circular obstruction we observed $L_c = -0.28973$ at meshing stage Q-1, and the drag coefficient is found $D_c = 8.3858$. The lift coefficient value at meshing level Q-1 is registered $L_c = 1.1978$ for triangular obstruction while the drag coefficient is observed $D_c = 5.0234$.



Hybrid meshing level Q-1.



Hybrid meshing level Q-6.

Figure 6. Meshing scheme for Event-II.

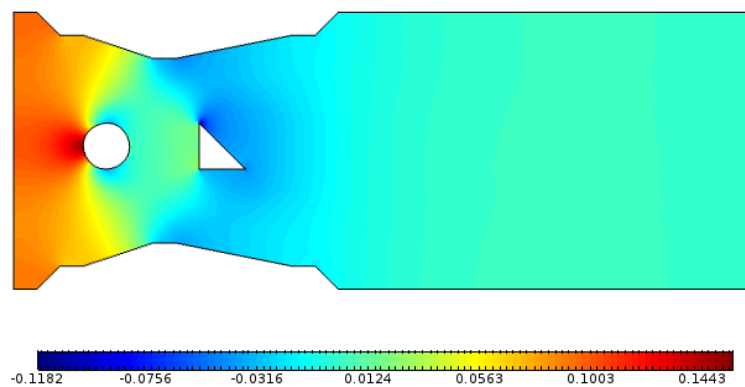


Figure 7. Pressure for circular/triangular event.

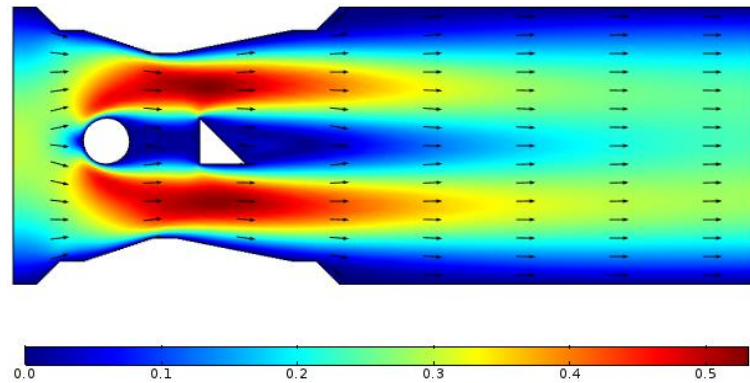


Figure 8. Velocity for circular/triangular event.

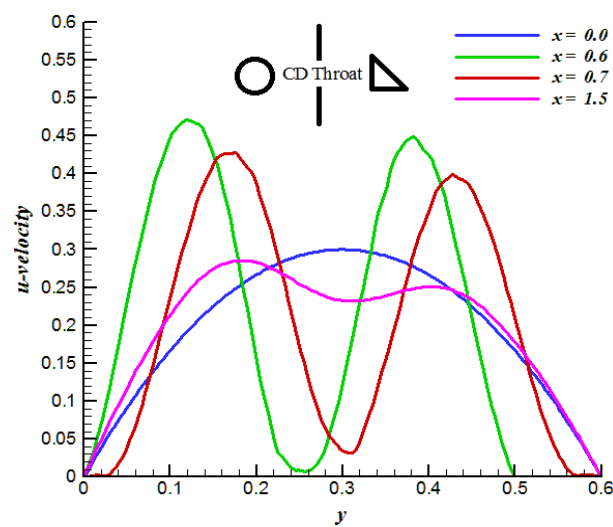


Figure 9. Line graph study for circular/triangular event.

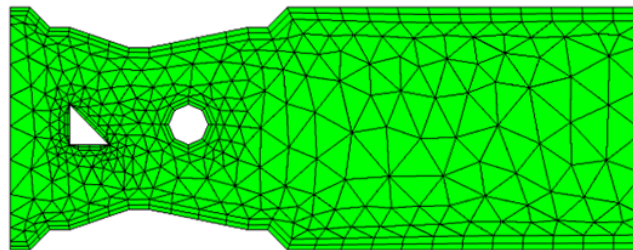
Table 5 offers the values of coefficients at different levels. Meshing level Q-6 has an accurate values. For the circular obstruction, we have $L_c = -0.19437$ and $D_c = 7.5651$. The values for the triangular obstacle are noted at level Q-6, that is drag coefficient $D_c = 4.5777$ and lift coefficient $L_c = 0.83949$. In comparison to the drag force faced by the triangular obstruction, the drag force faced by circular obstruction is greater in strength. The case of lift coefficient values is the reverse.

Table 5. Coefficients for circular/triangular event.

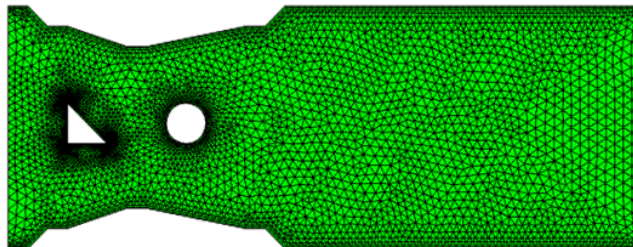
Levels (Q)	Circular obstacle in left vicinity		Triangular obstacle in right vicinity	
	Lift	Drag	Lift	Drag
1	-0.28973	8.3858	1.1978	5.0234
2	-0.27973	7.6259	0.93777	5.0978
3	-0.26225	7.6312	0.90315	4.8201
4	-0.25987	7.5594	0.84537	4.6973
5	-0.23774	7.5526	0.83966	4.6079
6	-0.19437	7.5651	0.83949	4.5777

5.3. EVENT-III. Triangular/circular as an obstruction in CD throat

We used the CD channel with triangular and circular-shaped hitches in this case. In the CD region, the triangular-shaped obstacle is installed, while the circular hitch is positioned in the CD channel region. The lateral length of the circular and triangular obstruction is 0.1m. To report the fluid in the CD domain, we used the FEM. Figure 10 gives the geometric description of the hybrid meshing of the channel with triangular/circular obstructions. The fluid field analysis of the CD domain that has triangular and circular obstacles is performed, see Figures 11–13. In concrete words, Figure 11 determines the pressure intensity for triangular and circular hitch. The fluid that communicates with the triangular barrier and the circular cylinder is found to have maximum left side strain. The pressure is strong in the convergence area of the CD channel. Figure 12 provides a fluid velocity distribution. The interaction of the fluid with the triangular obstruction allowed the fluid to rest compared to the triangular left side. The liquid has been bifurcated and such bifurcation moves around the CD throat to the circular obstacle mounted. The influence of cylinders on the fluid reduces dramatically down the stream.



Hybrid meshing level Q-1.



Hybrid meshing level Q-6.

Figure 10. Meshing scheme for Event-III.

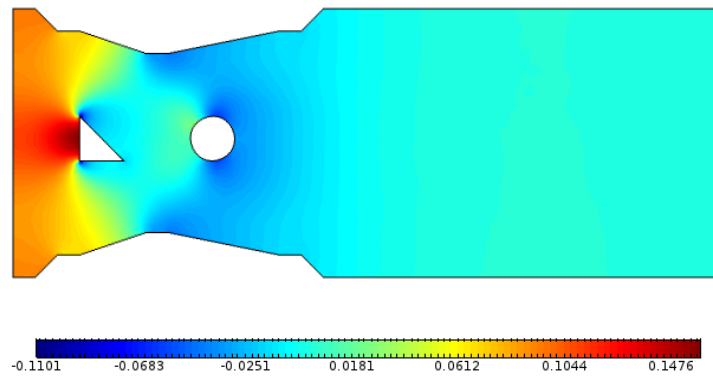


Figure 11. Pressure for triangular/circular event.

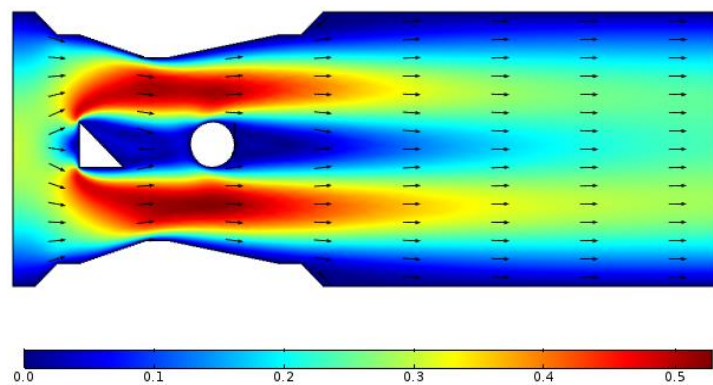


Figure 12. Velocity for triangular/circular event.

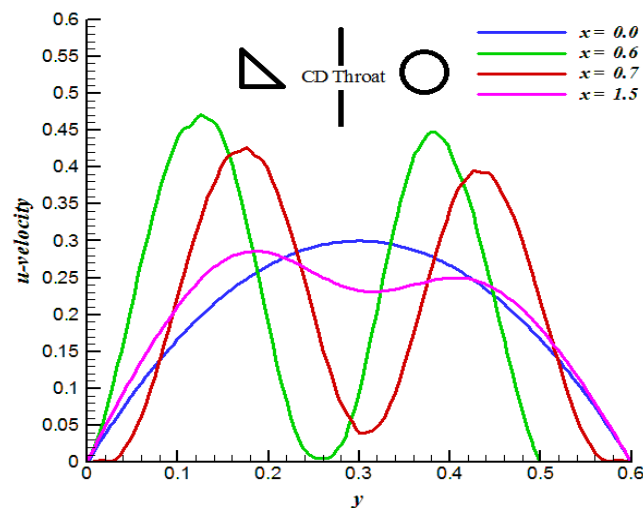


Figure 13. Line graph study for triangular/circular event.

The line graph analysis is carried out at unique channel positions to evaluate the frequency of u -velocity, see Figure 13. Parabolic profile is noted at $x = 0.0$. Fluid bifurcation is found at $x = 0.6$ and 0.7 in convergent-convergent regions. The fluid is seen to slow down at $x = 0.7$ as compared to $x = 0.6$. At $x = 1.5$ the velocity shows extreme low magnitude in comparison with rest of channel positions. Table 6 offers the lift coefficient $L_c = 0.51444$ for the triangular cylinder at hybrid meshing Q-1 while the drag

coefficient is noted $D_c = 10.141$. The lift coefficient for circular cylinder is reached $L_c = -0.42126$ and $D_c = 4.4931$ is the drag coefficient calculation. On level Q-6, the most positive value is indicated. The triangular cylinder drag coefficient is estimated $D_c = 9.1351$ and the lifting coefficient is calculated $L_c = 0.26593$. The circular cylinder lifting coefficient is found $L_c = -0.26189$. For circular cylinder we have drag coefficient $D_c = 4.0898$. In comparison with circular cylinder embedded in CD throat, the drag felt by the triangular cylinder is considerably strong. We made a comparison with Schäfer et al. [22] to gain confidence in our approach. We have taken into account the same dimensions as those mentioned in Ref. [22] for comparison. The considered rectangle has a length of 2.2 meters and a height of 0.41 meters. Fluid interact with circular obstacle positioned at (0.2, 0.2)m. At $Re = 20$, they observed the lift coefficient $C_L = 0.010618$ while the drag coefficient $C_D = 5.579535$. Table 7 offers the results comparison and we found an excellent match, which ensures the accuracy of the results at hand. The graphical comparison of lift and drag coefficients for present problem is offered by use of Figure 14a, b and Figure 15a, b. Such observations are reported for Event-I, Event-II, and Event-III. In detail, Figure 14a offers the drag coefficient values for obstructions in left locality for each event. We see that the drag faced by the triangular obstacle in Event-III is higher in magnitude. Figure 14b offers the drag coefficient values in the right vicinity of the throat for each event. It is seen that the drag coefficient for a triangular obstacle in Event-II is higher in magnitude. Figure 15a provides the comparative values of lift coefficient in the left vicinity of the throat for each case. One can see that at the improved meshing level, the lift coefficient is large in magnitude for a triangular obstacle in Event-III. Figure 15b offers the lift coefficient comparison for the right vicinity in each event. We observed that triangular obstruction possesses a higher value of lift coefficient for Event-I as compared to obstructions in Event-II and Event-III.

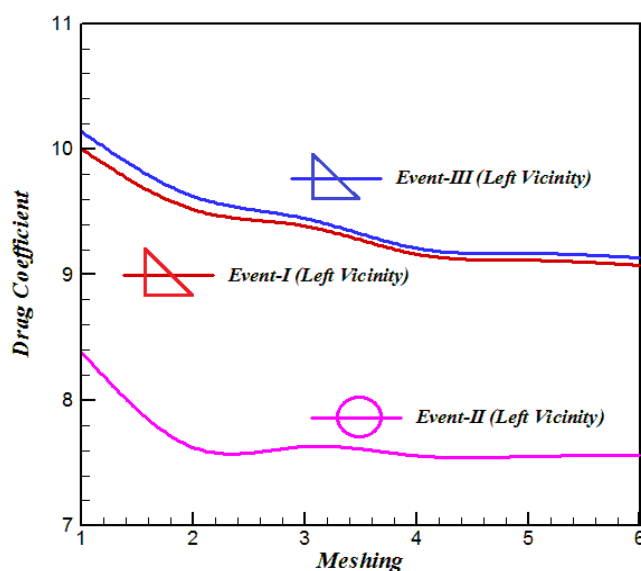


Figure 14(a). Drag coefficient comparison on obstructions in left vicinity.

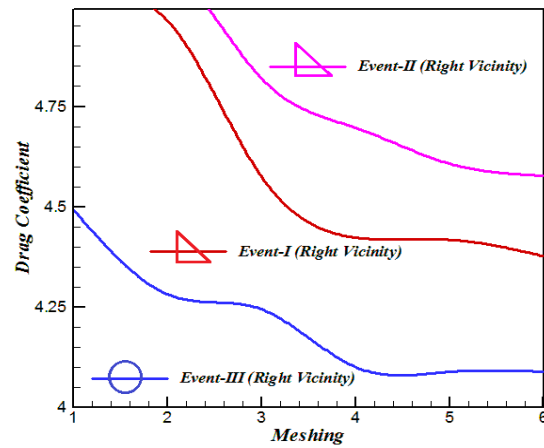


Figure 14(b). Drag coefficient comparison on obstructions in right vicinity.

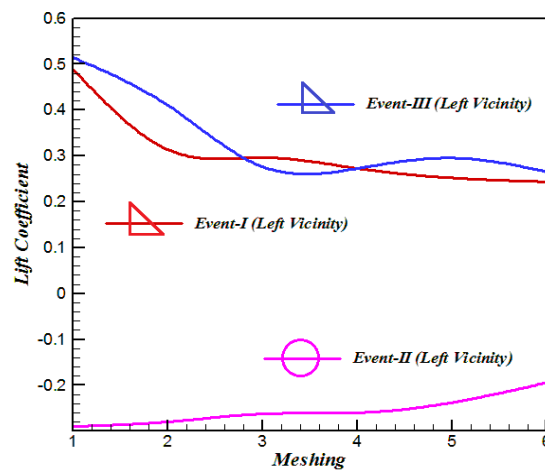


Figure 15(a). Lift coefficient comparison on obstructions in left vicinity.

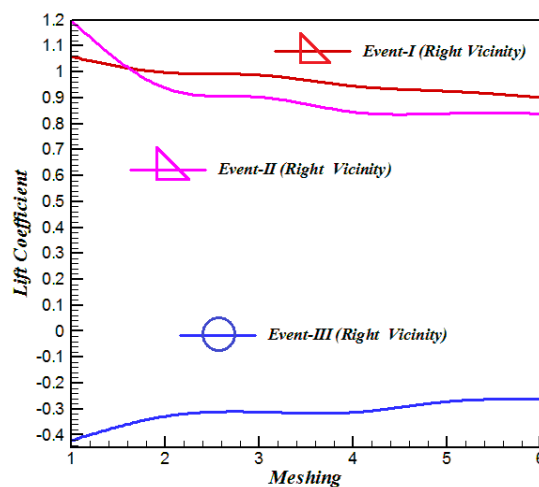


Figure 15(b). Lift coefficient comparison on obstructions in right vicinity.

Table 6. Coefficients for triangular/circular Event.

Levels (Q)	Triangular obstacle in left vicinity		Circular obstacle in right vicinity	
	Lift	Drag	Lift	Drag
1	0.51444	10.141	-0.42126	4.4931
2	0.41078	9.6253	-0.32821	4.2824
3	0.27694	9.4492	-0.31114	4.2452
4	0.27250	9.2101	-0.31305	4.1014
5	0.29564	9.1700	-0.27137	4.0892
6	0.26593	9.1351	-0.26189	4.0898

Table 7. Results comparison with Schäfer et al. [22]

Levels (Q)	Drag (Schäfer et al. [22])	Drag (Present Results)	Lift (Schäfer et al. [22])	Lift (Present Results)
1	-	6.5674	-	-0.06153
2	-	6.2789	-	-0.04367
3	-	5.9721	-	-0.03013
4	5.579535	5.5662	0.010618	0.02042
5	5.579535	5.5713	0.010618	0.01310
6	5.579535	5.5724	0.010618	0.01040

6. Conclusions

Motivated from Schäfer et al. [22], we offered optimized values of lift and drag coefficient for three different arrangements of obstacles in convergent-divergent channel. The alignment includes triangular/triangular, circular/triangular, and triangular/circular-shaped obstacles. The outcomes are obtained by using the finite element-based Comsol Multiphysics tool. The comparative analysis is itemized as follows:

- 1) The lift force faced by the triangular obstacle (in the left vicinity) shows inciting values for the coupling of the triangular obstacle (in the right vicinity) in comparison with the coupling of the circular obstacle (in the right vicinity).
- 2) The drag force reduces for triangular obstacle (in the left vicinity) when it gets coupled with a circular obstacle (in the right vicinity).
- 3) Owing to the left vicinity of the convergent-divergent channel, the lift force faced by the triangular cylinder is greater in magnitude.
- 4) The circular obstacle encountered greater drag in comparison to the drag force faced by the triangular impediment in the left vicinity.
- 5) The idea can be expanded to look at the hydrodynamic forces for non-Newtonian fluid flows around natural or manmade obstructions having engineering standpoints.

Acknowledgments

The authors would like to thank Prince Sultan University for their support through the TAS research lab.

Conflict of interest

The authors declare no conflict of interest.

References

1. J. H. Gerrard, An experimental investigation of the oscillating lift and drag of a circular cylinder shedding turbulent vortices, *J. Fluid Mech.*, **11** (1961), 244–256. <https://doi.org/10.1017/S0022112061000494>
2. S. C. Kacker, B. Pennington, R. S. Hill, Fluctuating lift coefficient for a circular cylinder in cross flows, *J. Mech. Eng. Sci.*, **16** (1974), 215–224. https://doi.org/10.1243/JMES_JOUR_1974_016_040_02
3. J. H. Gerrard, The wakes of cylindrical bluff bodies at low Reynolds number, *Philos. Trans. R. Soc. Lond. Ser. A Math. Phys. Sci.*, **288** (1978), 351–382.
4. C. Norberg, Flow around a circular cylinder: Aspects of fluctuating lift, *J. Fluids Struct.*, **15** (2001), 459–469. <https://doi.org/10.1006/jfls.2000.0367>
5. P. Catalano, M. Wang, G. Iaccarino, P. Moin, Numerical simulation of the flow around a circular cylinder at high Reynolds numbers, *Int. J. Heat Fluid Fl.*, **24** (2003), 463–469. [https://doi.org/10.1016/S0142-727X\(03\)00061-4](https://doi.org/10.1016/S0142-727X(03)00061-4)
6. M. Zhao, L. Cheng, B. Teng, D. F. Liang, Numerical simulation of viscous flow past two circular cylinders of different diameters, *Appl. Ocean Res.*, **27** (2005), 39–55. <http://doi.org/10.1016/j.apor.2004.10.002>
7. J. Deng, A. -L. Ren, J. -F. Zou, X. -M. Shao, Three-dimensional flow around two circular cylinders in tandem arrangement, *Fluid Dynam. Res.*, **38** (2006), 386. <http://doi.org/10.1016/j.fluidyn.2006.02.003>
8. M. M. Alam, Y. Zhou, Flow around two side-by-side closely spaced circular cylinders, *J. Fluids Struct.*, **23** (2007), 799–805. <https://doi.org/10.1016/j.jfluidstructs.2006.12.002>
9. T. Kitagawa, H. Ohta, Numerical investigation on flow around circular cylinders in tandem arrangement at a subcritical Reynolds number, *J. Fluids Struct.*, **24** (2008), 680–699. <http://doi.org/10.1016/j.jfluidstructs.2007.10.010>
10. M. C. Ong, T. Utnes, L. E. Holmedal, D. Myrhaug, B. Pettersen, Numerical simulation of flow around a smooth circular cylinder at very high Reynolds numbers, *Mar. Struct.*, **22** (2009), 142–153. <https://doi.org/10.1016/j.marstruc.2008.09.001>
11. S. Y. Cao, S. Ozono, Y. Tamura, Y. J. Ge, H. Kikugawa, Numerical simulation of Reynolds number effects on velocity shear flow around a circular cylinder, *J. Fluids Struct.*, **26** (2010), 685–702. <https://doi.org/10.1016/j.jfluidstructs.2010.03.003>
12. M. Zhao, L. Cheng, T. M. Zhou, Three-dimensional numerical simulation of oscillatory flow around a circular cylinder at right and oblique attacks, *Ocean Eng.*, **38** (2011), 2056–2069. <https://doi.org/10.1016/j.oceaneng.2011.09.007>
13. M. S. Akoz, Investigation of vortical flow characteristics around a partially buried circular cylinder, *Ocean Eng.*, **52** (2012), 35–51. <https://doi.org/10.1016/j.oceaneng.2012.06.011>

14. L. -H. Yu, J. -M. Zhan, Y.-S. Li, Numerical investigation of drag force on flow through circular array of cylinders, *J. Hydrodyn.*, **25** (2013), 330–338. [https://doi.org/10.1016/S1001-6058\(11\)60371-6](https://doi.org/10.1016/S1001-6058(11)60371-6)
15. O. Lehmkuhl, I. Rodríguez, R. Borrell, J. Chiva, A. Oliva, Unsteady forces on a circular cylinder at critical Reynolds numbers, *Phys. Fluids*, **26** (2014), 125110. <https://doi.org/10.1063/1.4904415>
16. H. Mehdi, V. Namdev, P. Kumar, A. Tyagi, Numerical analysis of fluid flow around a circular cylinder at low Reynolds number, *IOSR J. Mech. Civil Eng.*, **3** (2016), 94–101. <http://doi.org/10.9790/1684-13030294101>
17. D. -L. Gao, W. -L. Chen, H. Li, H. Hu, Flow around a circular cylinder with slit, *Exp. Therm. Fluid Sci.*, **82** (2017), 287–301. <https://doi.org/10.1016/j.expthermflusci.2016.11.025>
18. Z. Z. Bao, G. L. Qin, W. Q. He, Y. Z. Wang, Numerical investigation of flow around a slotted circular cylinder at low Reynolds number, *J. Wind Eng. Ind. Aerod.*, **183** (2018), 273–282. <https://doi.org/10.1016/j.jweia.2018.11.010>
19. A. Escobar, V. Negro, J. S. López-Gutiérrez, M. D. Esteban, Influence of temperature and salinity on hydrodynamic forces, *J. Ocean Eng. Sci.*, **1** (2016), 325–336. <https://doi.org/10.1016/j.joes.2016.09.004>
20. H. X. Zheng, J. S. Wang, Efficient three-dimensional high-resolution simulations of flow fields around cylinders, *J. Ocean Eng. Sci.*, **3** (2018), 205–217. <https://doi.org/10.1016/j.joes.2018.08.001>
21. A. Najafi, H. Nowruzi, On hydrodynamic analysis of stepped planing crafts, *J. Ocean Eng. Sci.*, **4** (2019), 238–251. <https://doi.org/10.1016/j.joes.2019.04.007>
22. M. Schäfer, S. Turek, F. Durst, E. Krause, R. Rannacher, Benchmark computations of laminar flow around a cylinder, In: *Flow Simulation with High-Performance Computers II*, 1996, 547–566. https://doi.org/10.1007/978-3-322-89849-4_39
23. R. Mahmood, N. Kousar, K. Usman, A. Mehmood, Finite element simulations for stationary Bingham fluid flow past a circular cylinder, *J. Braz. Soc. Mech. Sci. Eng.*, **40** (2018), 459. <http://doi.org/10.1007/s40430-018-1383-2>
24. K. U. Rehman, M. S. Alqarni, R. Mahmood, N. Kousar, M. Y. Malik, A classical remark on the compatibility of inlet velocity and pressure singularities: Finite-element visualization, *Eur. Phys. J. Plus*, **134** (2019), 230. <http://doi.org/10.1140/epjp/i2019-12628-8>
25. Y. -M. Chu, M. S. Hashmi, N. Khan, S. U. Khan, M. I. Khan, S. Kadry, et al., Thermophoretic particles deposition features in thermally developed flow of Maxwell fluid between two infinite stretched disks, *J. Mater. Res. Technol.*, **9** (2020), 12889–12898. <https://doi.org/10.1016/j.jmrt.2020.09.011>
26. M. Nazeer, F. Hussain, M. I. Khan, A. -U. Reham, E. R. El-Zahar, Y. -M. Chu, et al., Theoretical study of MHD electro-osmotically flow of third-grade fluid in micro channel, *Appl. Math. Comput.*, **420** (2022), 126868. <http://doi.org/10.1016/j.amc.2021.126868>
27. K. U. Rehman, E. A. Algehyne, F. Shahzad, E. -S. M. Sherif, Y. -M. Chu, On thermally corrugated porous enclosure (TCPE) equipped with casson liquid suspension: Finite element thermal analysis, *Case Stud. Therm. Eng.*, **25** (2021), 100873. <https://doi.org/10.1016/j.csite.2021.100873>

28. Introduction to COMSOL multiphysics®, In: *COMSOL Multiphysics*, Available from: https://cdn.comsol.com/doc/6.1.0.282/IntroductionToCOMSOLMultiphysics.zh_CN.pdf
29. A. Pishkoo, M. Darus, Using fractal calculus to solve fractal Navier-Stokes equations, and simulation of laminar static mixing in COMSOL Multiphysics, *Fractal Fract.*, **5** (2021), 16. <https://doi.org/10.3390/fractalfract5010016>
30. A. A. Memon, M. A. Memon, K. Bhatti, K. Jacob, T. Sitthiwirattam, C. Promsakon, et al., Modelling and simulation of fluid flow through a circular cylinder with high Reynolds number: A COMSOL multiphysics study, *J. Math.*, **2022** (2022), 5282980. <https://doi.org/10.1155/2022/5282980>



AIMS Press

© 2023 the Author(s), licensee AIMS Press. This is an open access article distributed under the terms of the Creative Commons Attribution License (<http://creativecommons.org/licenses/by/4.0>)